Photochemical & Photobiological Sciences

PERSPECTIVE

Cite this: *Photochem. Photobiol. Sci.*, 2016, **15**, 714

# Microfluidic-based photocatalytic microreactor for environmental application: a review of fabrication substrates and techniques, and operating parameters

Susmita Das and Vimal Chandra Srivastava*

Received 28th December 2015,
Accepted 21st April 2016

DOI: 10.1039/c5pp00469a

www.rsc.org/pps

Photochemical technology with microfluidics is emerging as a new platform in environmental science. Microfluidic technology has various advantages, like better mixing and a shorter diffusion distance for the reactants and products; and uniform distribution of light on the photocatalyst. Depending on the material type and related applications, several fabrication techniques have been adopted by various researchers. Microreactors have been prepared by various techniques, such as lithography, etching, mechanical microcutting technology, *etc*. Lithography can be classified into photolithography, soft lithography and X-ray lithography techniques whereas the etching process is divided into wet etching (chemical etching) and dry etching (plasma etching) techniques. Several substrates, like polymers, such as polydimethyl-siloxane (PDMS), polymethyle-methacrylate (PMMA), hydrogel, *etc.*; metals, such as stainless steel, titanium foil, *etc.*; glass, such as silica capillary, glass slide, *etc.*; and ceramics have been used for microchannel fabrication. During degradation in a microreactor, the degradation efficiency is affected by few important parameters such as flow rate, initial concentration of the target compound, microreactor dimensions, light intensity, photocatalyst structure and catalyst support. The present paper discusses and critically reviews fabrication techniques and substrates used for microchannel fabrication and critical operating parameters for organics, especially dye degradation in the microreactor. The kinetics of degradation has also been discussed.

## 1. Introduction

Photocatalysis has become a very common technique in various disciplines such as in chemical synthesis, environmental technology and medicine.[1] Traditionally, photocatalytic degradation is carried out in batch mode with a light source kept at the top of the reactor, and a catalyst is used in the form of dispersed powder. This configuration provides a non-uniform distribution of UV light which reduces the reaction efficiency[2–5] and the costly separation of the catalyst is necessary after the reaction. In any practical situation, immobilization of the catalyst is preferred to minimize the experimental costs.[6,7] Problems associated with the non-uniformity of light and the immobilization of catalyst could be resolved by using a microreactor. Microreactors with very small channel dimensions (a few hundred microns) provide uniform exposure of light to all of the contaminated water present in the microreactor.[1] Catalyst immobilization within microchannels helps in the utilization of the catalysts' large surface to volume ratio. In light of the several advantages of a microreactor, contaminants get significantly degraded within a few seconds, which occurs in several hours in bulky reactors.[8–10] A number of researchers have carried out photochemical reactions within microchannels without using any catalyst, such as the photochemical coupling of benzophenone to benzopinacol,[11] singlet oxygen production,[12] and the photochemical chlorination of alkylaromates.[13] Photocatalytic degradation within microreactors has also been carried out using several immobilized catalysts such as $TiO_2$, ZnO and Pt/ZnO[14–16] for the degradation of different dyes like methylene blue and methyl orange. Typically, microchannels are prepared using different substrates such as polydimethyl-siloxane (PDMS), polymethyl-methacrylate (PMMA), silicon, glass and alumina, depending on its application.[17–19] Biocompatible materials, silicon and glass have also been used as substrates for microchannel fabrication by photolithography and chemical etching processes.[20–22] Several issues are involved with these materials, such as the requisition of specialized tools, the long preparation time and higher manufacturing cost. PDMS is one such alter-

*Department of Chemical Engineering, Indian Institute of Technology Roorkee, Roorkee, 247667 Uttarakhand, India. E-mail: vimalcsr@yahoo.co.in, vimalfch@iitr.ac.in, susmita.82.das@gmail.com; Fax: +91-1332-276535; Tel: +91-1332-285889*

native substrate, which is biocompatible, flexible and has shown excellent optical performance which resolves several issues.[23–28]

In the literature, several reviews have been published in the field of photochemical degradation of dyes in laboratory scale batch reactors,[29–32] however, reviews on work done in photochemical microreactors are scarce. This paper intends to aid researchers involved in the photochemical treatment of dyes within microreactors by compiling data on the microchannel fabrication method, factors influencing dye degradation within microchannels, reaction mechanisms, and summarizing and discussing data on materials used for microchannel fabrication, the catalysts used, and dyes photodegraded during the process.

## 2. Mechanism of photocatalytic reaction

Photocatalytic reactions occur under UV or visible light irradiation with the help of a metal oxide catalyst, like $TiO_2$, ZnO, $Fe_2O_3$, $SnO_2$, $SiO_2/TiO_2$, *etc*.[33–35] Photocatalytic degradation occurs by producing a hydroxyl radical, which is a very powerful oxidant with an oxidation potential of 2.8 V (NHE), as per the following reactions:

$$\text{Metal oxide catalyst} + h\nu \rightarrow {e_{CB}}^- + {h_{VB}}^+ \quad (1)$$

$$e^- + O_2 \rightarrow {}^\bullet{O_2}^- \quad (2)$$

$${}^\bullet{O_2}^- + HO_2{}^\bullet + H^+ \rightarrow H_2O_2 + O_2 \quad (3)$$

$$h^+ + H_2O \rightarrow {}^\bullet OH + H^+ \quad (4)$$

$$h^+ + OH \rightarrow {}^\bullet OH \quad (5)$$

$${}^\bullet OH + \text{organic compounds} \rightarrow \text{intermediates} \rightarrow \text{products} \quad (6)$$

The valence band (VB) electrons of the catalyst are promoted to the conduction band (CB) to generate electron–hole pairs by absorbing a photon with an energy equal to or greater than the band gap energy under irradiation *via* eqn (1).[36–38] The generated negative electrons at the conduction band form hydrogen peroxide by reducing dissolved oxygen to superoxide radical anions *via* eqn (2) and (3).[39] Positive holes at the valence band produce hydroxyl radicals from adsorbed water or hydroxide ions by oxidization *via* eqn (4) and (5).[40] At or near the surface of the catalyst, the produced hydroxyl radicals degrade the organic compounds to its final products following the production of intermediates, as per eqn (6).

Photocatalysts have been modified by different mechanisms, such as non-metal doping,[41] metal or metal ion incorporation[42] and carbon nanotube coupling[43] to enhance their photocatalytic response. Recombination of electron–hole pairs is the major limitation in photocatalysts which reduces the overall efficiency. This problem could be solved by adding an electron acceptor which helps in scavenging excited electrons.[44]

Various types of non-metals, such as nitrogen, fluorine, carbon, phosphorous and sulfur, have been used as a dopant on photocatalysts to enhance the photocatalytic activity under UV irridiation.[45–48] Non-metallic anionic dopants improve the stability and activity of the doped photocatalyst better than metal dopants.[49] These dopants form a new impurity level near the valence band while maintaining the large band gap, thus improving the degradation efficiency. Therefore, a number of investigators have used anion-doped photocatalysts for visible-light activated photocatalysis in recent years.[48,50–53] It may be noted that the crystalline and porous nature, and the crystal size of the photocatalysts decreased with an increase in doping.[52,54]

**Susmita Das**

*Dr Susmita Das received her PhD in Chemical Engineering from Indian Institute of Technology (IIT) Kanpur in 2013. She was guest faculty in the department of Polymer and Process Engineering, IIT Roorkee for one semester. After a post-doctorate position at IIT Roorkee during 2014–2015, she joined the Department of Chemical Engineering, IIT Roorkee, as a Young Scientist Fellow. During her PhD, she worked on bioinspired fracture mechanics, and her current research interests include environmental science (specifically waste water treatment), catalysis, and nanoparticle synthesis and characterization.*

**Vimal Chandra Srivastava**

*Dr Vimal Chandra Srivastava is Associate Professor in the Department of Chemical Engineering, IIT Roorkee, India. His major research interests are: industrial pollution abatement, desulfurization, catalysis, $CO_2$ utilization, alternative fuels, adsorption, electro-chemical methods and nanoparticle synthesis. He has authored >120 papers, 5 book chapters and has received 4500 citations of his papers with an* h*-index of 32. He has guided 8 PhD and 40 MTech students. He was awarded Prosper.Net-SCOPUS Young Researcher Award 2010 – First Runner-up Prize, INAE Young Engineer Award 2012, INSA Young Scientist Medal 2012, IE Young Engineer Award 2013 and IIChE-Amar Dye-Chem Award 2013.*

# 3. Fabrication of microfluidic devices

## 3.1 Materials

Microchannels have been fabricated using various types of materials, such as polydimethyl siloxane (PDMS),[55] polymethyl methacrylate (PMMA),[56] polystyrene (PS),[57] polyethylene terephthalate (PET),[58] quartz,[59] silicon,[60] photostructured glass ceramic[61] and stainless steel,[62] *etc*. depending upon the application.

## 3.2 Methods

Depending on the material type and related applications, several fabrication techniques have been adopted by several researchers. In the next section, we discuss some important and most widely used microchannel fabrication techniques.

Microchannels have been fabricated using several techniques. Lithography is one of the most often used technique.[63–67] Lithography can be classified into photolithography, soft lithography and X-ray lithography. The photolithography technique involves several steps such as wafer cleaning, barrier layer formation, soft baking, mask alignment, exposure and development, and hard-baking.[68] Initially, a wafer is chemically cleaned by hydrogen peroxide and a barrier layer of silicon dioxide is formed on the wafer surface. A thin uniform layer of positive or negative photoresist is developed on the silicon dioxide formed wafer surface by spin coating under UV exposure. A negative photoresist is formed with the help of a mask. Soft baking is used to remove the uppermost layer of the substrate in the areas that are not protected by the photoresist. After soft baking, a pattern is transferred to the photoresist by shining light through the mask, and is finalized by hard-baking steps. Researchers like Choi *et al.*[68] and Arayanarakool *et al.*[69] have prepared microchannels using photolithography technique. The soft lithography technique uses a pattern elastomer as a mask, stamp, or mold to generate micropatterns and microstructures instead of using a rigid photomask. This technique includes replica molding, micro-contact printing, micromolding in capillaries and micro-transfer molding.[70] This technique consists of a positive silicon master or stamp where polymeric elastomers are casted and cured. After curing, the elastomeric polymer is peeled off the stamp and by using this silicon stamp, hundreds of polymeric microfluidic devices are replicated. The soft lithography technique has several advantages, such as the short turnaround time and low cost, and it is applicable to almost all polymers and the bonding of polymers to each other, or to glass or plastic substrate using a conformal contact.[69] A disadvantage of this technique is the swelling which occurs because of nonpolar solvents (toluene, hexane) and the deformation of the soft elastomeric stamp.[70] The X-ray lithography technique uses X-rays to transfer a pattern on a light sensitive photoresist on a silicon substrate. The limitation of this process is the higher cost of manufacturing which restricts its wide usage.[71–74]

A non-lithographic technology, called 3-D printing technology, has also been used for microchannel fabrication, which is low in cost and environment friendly.[75] In this process, computer-aided design (CAD) software is used to design a 3-dimensional pattern on the surface of a smooth paper using a solid ink printer or laser jet printer. Organic solvents are used as ink for printing purposes. In general, after the formation of the 3-D pattern, the polymer is replicated by a curing process to form negative relief channels. Finally, a negative polymeric mold is attached to a flat substrate to form a microfluidic device. Importantly, the inlet and outlet connector of the microchannel is fabricated directly by the mold, which reduces the cost of drilling and eliminates the possibilities of crack formation in the cured polymer.

Martinez *et al.*[76] introduced for the first time microfluidic paper-based analytical device (μPAD) technology, in which hydrophobic materials, such as wax and polymer, are patterned on hydrophilic paper. Martinez and co-workers[76–84] further reported a number of advantages, such as the non-requirement of active pumping, and the reproducibility and sensitivity of the technology for various applications with respect to biological samples.[85] A number of new patterning techniques such as laser,[86,87] wax,[77,78,81,88–90] inject printing,[91] plasma etching,[92,93] cutting,[94] mechanical plotting,[86] and Sharpie ink permanent markers[95] have further been developed. Paper microfluidics have been successfully applied in a number of biological and biochemical applications.[96–99]

The etching process is another commonly used technique for microchannel fabrication, where a pattern is formed by physically or chemically removing material or layers from the substrate. In general, the etching process is divided into two classes: wet etching (chemical etching) and dry etching (plasma etching) techniques. In the wet etching process, a patterned mask is deposited on the wafer using a lithography technique to protect the required surface, and the unprotected area is removed by liquid chemical or etchant.[94] The dry etching process uses high energy kinetic energy beams (physical etching) or liquid etchants (chemical etching) or both together to remove the substrate.[100] Microchannel fabrication by a dry etching process is more efficient than the wet etching process.[101,102]

Furthermore, mechanical microcutting technology is another process which can fabricate microchannels from a wide range of materials *e.g.* aluminum, steel, brass, plastics and polymers. Micromilling and microturning processes are the most used processes within mechanical cutting technology. High machining speed, a good surface finish, and a high level of machining accuracy can be achieved using ultra-precision machine tools.[103] The disadvantages include long procession time, crack generation and the erosion of cutting tools.

Microchannels have also been fabricated by introducing spacers or string within a substrate. Hakamada *et al.*[104] fabricated microchannels on metal bodies (copper) using a spacer method. The inner diameters of microchannels have been varied using different spacer sizes. Verma *et al.*[105] fabricated polymeric microchannels by PDMS (poly dimethylsiloxane) by introducing a nylon thread within it. By using this method, various orientations like knots, helices, super-helices, and other varieties of channel cross-sections have been fabricated.

 

# 4. Microfluidics in photocatalytic applications

Several substrates, like polymers, such as PDMS, PMMA and hydrogel, *etc.*; metals, such as stainless steel, titanium foil, *etc.*; glass, such as silica capillary, glass slide, *etc.*; and ceramics have been used for microchannel fabrication. In the following section, a few important photocatalytic microchannels made of different substrates have been discussed briefly.

## 4.1 Polymeric microreactor

**4.1.1. PDMS.** Meng *et al.*[19] fabricated a microfluidic based photocatalytic microreactor made of a biocompatible PDMS substrate for the degradation of methylene blue (MB) dye solution, as shown in Fig. 1. A PDMS microchannel of 100 mm depth, 500 mm width was fabricated with the help of a SU-8 template using soft lithography technique, and sealed with glass substrate to form a closed microchannel. A nanofibrous $TiO_2$ photocatalyst, synthesized by an electrospinning and calcination technique, was kept within the microchannel before sealing. The photocatalytic efficiency of the nanofibrous $TiO_2$ microreactor was higher than that of bulk and $TiO_2$ film microreactors. This was because highly porous structure of the nanofibrous $TiO_2$ provided a large surface area, whereas the $TiO_2$ film reactor only provided a limited contact area. Lamberti *et al.*[106] proposed a PDMS microchannel by casting and replication technology for the photocatalytic degradation of MB. Using a conventional dip coating and subsequent drying method, a $TiO_2$ nanoparticle film was formed on a glass substrate. A prepolymeric PDMS mixture was poured on the film coated glass substrate which was removed after curing the PDMS to form a $TiO_2$/PDMS membrane. Another PDMS template with an inlet and outlet system was attached to a PDMS membrane to form a microfluidic device. Very high photocatalytic degradation efficiency (100%) of MB was achieved within 6 min using the $TiO_2$ NPs incorporated on the PDMS surface microfluidic device. Han *et al.*[107] prepared a microfluidic device using soft lithography technique for the photodegradation of organic dye methylene blue. A ZnO seed layer was used to prepare ZnO nanowires (NWs) on a glass substrate using hydrothermal process. A standard photolithography technique was used to prepare a SU-8 3050 photoresist patterned mask which was replicated on PDMS by a casting method. Finally, PDMS and a glass substrate with thermally grown ZnO NWs were bonded together by plasma oxidation to prepare a microreactor. The ZnO NWs integrated microfluidic device showed 96% dye degradation, whereas only ~34% of MB was degraded by the conventional method with dispersed ZnO NWs under the same UV irradiation. Rasponi *et al.*[108] prepared a PDMS micro photocatalytic cell using soft lithography technique. A rectangular cross-sectioned channel of dimensions 4.5 mm wide × 25 mm long × 0.1 mm high was plasma bonded with a pretreated quartz slice. The quartz wafer was treated with a $TiO_2$ thin film followed by a 200 nm indium tin oxide thin film using reactive radio-frequency sputtering. The bias potential was maintained by exposing a platinum (Pt) electrode to the liquid flowing into the channel. Photocatalytic degradation of the dye was carried out at different flow rates and under bias voltages ranging from no bias to 5 V bias. At 5 V bias voltage, ~95% color removal was achieved, whereas for no bias voltage condition, about 20% color removal was achieved in 150 s. Results also showed that irrespective of the bias voltage, MB degrades exponentially with residence time.

**4.1.2. PMMA.** Eskandarloo and Badiei[109] fabricated rectangular microchannels of dimensions 400 μm width, 50 μm depth, and 80 cm length, inscribed by a simple and inexpensive $CO_2$ laser technique on a PMMA plate. The microchannel turns 12 times within a 30 mm length. A $TiO_2$ catalyst was deposited within the bottom and two side walls of the microchannel by a heat attachment method. The catalyst immobilized PMMA plate was covered with quartz glass, followed by sandwiching between a cover and housing plates to form a microreactor. Textile dyes like methyl orange, acid violet 19, malachite green, acid orange 7 and basic red 46 were used as pollutants. This investigation showed that higher photocatalytic degradation is achieved at lower flow rates, lower inlet concentrations, higher light intensities, and longer microchannel lengths.

**4.1.3. Hydrogel.** Koo and Velev[110] prepared a biomimetic photocatalytic reactor for MB degradation inspired by the structure and material composition of natural leaves. The

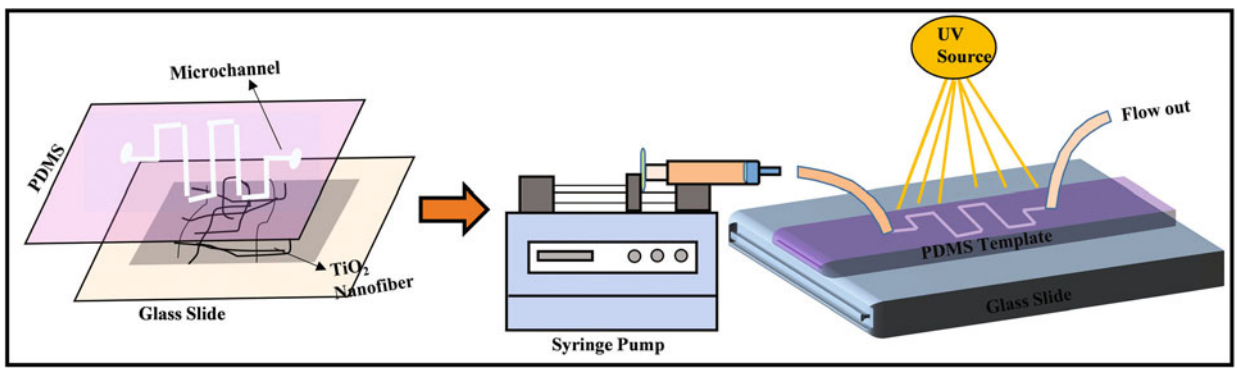


Fig. 1 Schematic of microreactor experimental setup used by Meng *et al.*[19]

liquefied agarose with suspended $TiO_2$ nanoparticles was replicated using a patterned SU-8 mold to obtain branched channel network in the hydrogel. Finally, the replicated hydrogel was enclosed in a PDMS spacer, followed by sandwiching between two glass substrates. An inlet and outlet system was maintained by inserting pieces of Tygon tubing.

**4.1.4. Epoxy resin.** Charles *et al.*[111] fabricated rectangular microchannel reactors in an epoxy resin using a home-made stereo-lithography apparatus using a UV Nd-YAG laser for the photocatalytic degradation of an aqueous solution of salicylic acid. In this process, liquid resin was converted to a solid polymer by laser radiation and the consequent curing of successive layers of resin formed a three-dimensional microreactor. The microreactor inner surface (only the two side walls and the bottom of the channel) was coated with $TiO_2$ photocatalyst by several experimental steps. Finally, the $TiO_2$ coated microreactor was sealed with a glass top plate using an epoxy glue. An aqueous solution of salicylic acid was passed through the microchannel with a syringe. Experiments were carried out at different flow rates, initial concentrations, microchannel sizes, and incident UV light intensities. The results showed that the catalytic degradation was higher at lower flow rates, lower initial concentrations and higher incident light intensities. A monomolecular Langmuir–Hinshelwood kinetics method was used to determine the kinetics of photocatalytic reaction. Corbel *et al.*[112] fabricated an epoxy resin microchannel with a rectangular cross-section of about 1 $mm^2$ and a length of 70 mm with different aspect ratios defined as width/depth using a stereolithography technique. Salicylic acid (SA) was used as a pollutant model in order to evaluate the influence of the radial concentration profile of the microchannel on the photocatalytic degradation efficiency. The inner bottom wall of the microchannel was coated with a $TiO_2$ catalyst and the photodegradation of SA was tested in different geometric configurations. The better photocatalytic activity was achieved for the microchannel with the shallowest depth and the highest surface specific area. The degradation experiments were carried out with different dye concentrations and different flow rates. The investigation showed that 65% of pollutant degradation was found at optimum conditions with the pollutant concentration equal to 0.07 mol $m^{-3}$ and a flow rate of 2 mL $h^{-1}$.

**4.1.5. Inorganic polymer (allylhydridopolycarbosilane).** Yoon *et al.*[113] reported an optically transparent glass-like inorganic polymeric (allylhydridopolycarbosilane) microreactor prepared using a UV imprinting lithography technique. 4-Chlorophenol was used as a pollutant for photocatalytic degradation with a $TiO_2$ photocatalyst. Experiments were carried out with conventional glass and an inorganic polymeric reactor with $TiO_2$ coated microbeads by a sol–gel method. The analysis showed the better performance of the inorganic polymer microreactor as compared to the commercial glass microreactor.

### 4.2 Glass microreactor

**4.2.1. Glass.** Lei *et al.*[114] demonstrated a rectangular microfluidic photocatalytic reactor of dimensions 5 cm × 1.8 cm × 100 μm, which was constructed by two porous $TiO_2$-coated glasses as the top cover and bottom substrate for the treatment of MB dye using solar energy. By using a standard UV lithography technique, a template of Norland Optical Adhesive (NOA81) was replicated from a PDMS mold, which was further used as a spacer and sealant in between the two porous $TiO_2$-coated glass slides. The porous $TiO_2$ films were prepared on the glass surface using a sol–gel method. The effects of reactor parameters such as film preparation methods, thickness of $TiO_2$ films, and flow rates were studied. Experiments showed that the microreactor with $TiO_2$ exhibited faster dye degradation than the bulk container. Lindstrom *et al.*[115] described microfluidic devices made of soda-lime glass blank wafers which were used for MB degradation under UV radiation. Microchannels were prepared on 15 mm soda-lime glass blank wafers which were pre-coated with low reflective chromium and photoresist using a direct write laser lithography and wet etching method. The channels of the devices were coated with a layer of $TiO_2$ nanoparticles. 99.9% MB degradation was observed at a flow rate of 3 ml $min^{-1}$ under UV exposure. Ramos *et al.*[116] photocatalytically degraded methylene blue dye within a commercially available borosilicate glass microreactor with a semi-elliptic microchannel of dimensions 100 μm × 40 μm × 50 cm under UV-LED-irradiation. The $TiO_2$ catalyst was immobilized within microchannels using a sol–gel method. Experiments were performed with and without $TiO_2$ catalyst, and the results showed that decolorization was higher in the presence of the photocatalytic layer.

**4.2.2. Silica capillary.** Tsuchiya *et al.*[3] studied the photocatalytic degradation of several typical dyes in a microreactor by monitoring their fluorescence spectra. A transparent fused silica capillary was coated to a thickness of 0.3 microns with $TiO_2$ solution, and dyed to get a 0.3 micron thickness. Experiments were carried out with aqueous solutions of different dyes, such as sunset yellow, new coccine, methyl red, rhodamine 6G, methylene blue and erythrosine. Time-dependent responses which were observed by experiments have been reproduced by simulations based on models of the reaction kinetics. The photocatalytic reaction kinetics was analyzed by pseudo-first-order or Langmuir–Hinshelwood models. He *et al.*[117] fabricated a novel, highly durable, $TiO_2$ nanoparticle-coated, ZnO nanorod array coated silica glass capillary-based photocatalytic microreactor (Fig. 2). Silica glass capillaries with a polyimide outer coating were used as the microchannels. $TiO_2$ nanoparticle-coated ZnO nanorod arrays were grown on the inner wall of the capillary by pumping a $TiO_2$ solution into capillaries containing preformed ZnO nanorod arrays. Photocatalytic degradation of methylene blue was performed within the capillary microreactors (CMs). At a particular residence time, CMs with ZnO/$TiO_2$ nanorod arrays showed enhanced photocatalytic performance compared to the CMs containing pristine ZnO nanorods. At RT = 20 s, CMs containing ZnO/$TiO_2$-3 ($TiO_2$ was coated 3 times) showed 100% degradation. After repeated use for 100 h, the microreactor showed more than 90% efficiency. Coupled semiconductor nanocomposites increased the surface area of the capillary microreactor and

 

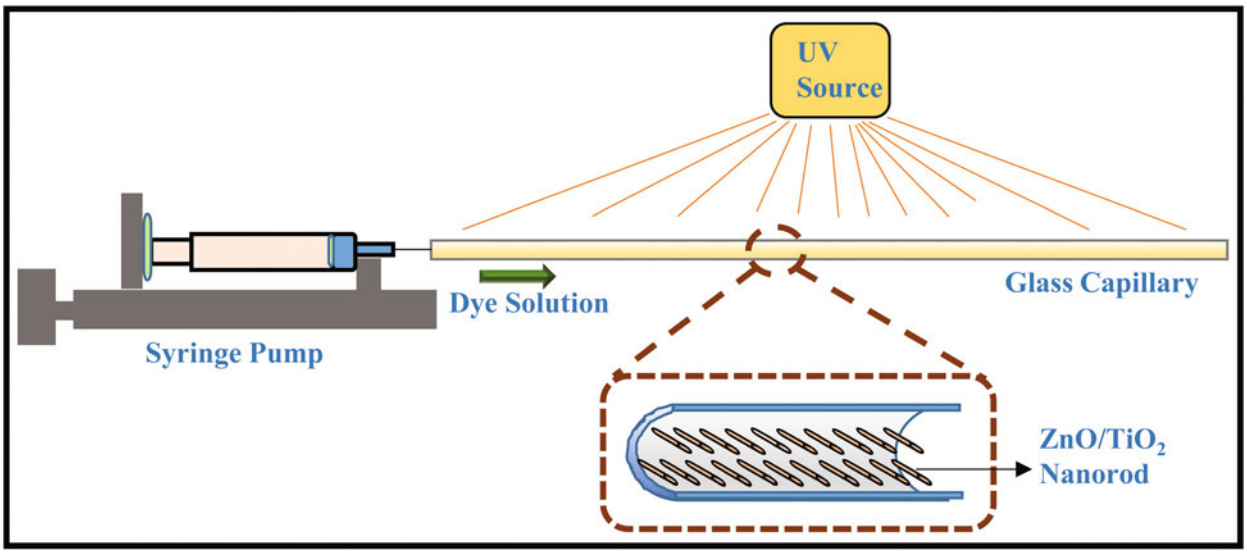


Fig. 2 Schematic of experimental set up of a capillary microreactor used by He *et al.*[117]

accelerated photogenerated electron transport due to their structural properties. Li *et al.*[118] used a microreactor of silica capillaries of length 5 cm, and 530 and 200 μm inner diameters with a glass inner wall. The inner surface of the channel was modified by $SiO_2/TiO_2$ colloid solution. Irrespective of the channel inner diameter, the $SiO_2/TiO_2$ coated microreactor showed higher conversion than the $TiO_2$ coating alone or without coating under the same UV irradiation. The results showed that the dye degradation rate increased by more than 150 times for the $SiO_2/TiO_2$ modified micro-space compared to that of a batch system. Nakamura *et al.*[119] prepared a 5 cm long silica-glass capillary microreactor with an inner diameter of 530 cm with a glass inner wall and polyimide coated outside for the degradation of methylene blue. Experiments were performed with a $TiO_2$ or $SiO_2/TiO_2$ modified microreactor, a non-treated microreactor and a batch reactor under UV irradiation. The batch reactor degraded dye at a very low reaction rate of about 0.09% $s^{-1}$ within 60 min, whereas the microreactor (530 μm capillary) of $SiO_2/TiO_2$-coated reduced the dye at a fairly rapid rate of 5.7% $s^{-1}$ for complete degradation within 40–50 s. Irrespective of the type of microreactor, a smaller diameter microchannel showed better performance in dye degradation. In the above studies, syringe pumps were used to pump the contaminant solution within a single capillary microchannel. Other researchers, like Shen *et al.*,[15] Zhang *et al.*,[16] and Oda *et al.*[120] demonstrated similar kinds of microreactor for the photocatalytic degradation of methyl orange, phenol and rhodamine 6G, respectively.

There are few examples of capillary microchannels where the pollutant solution goes inside the capillary by the capillary force itself without using a syringe pump. For example, Katayama *et al.*[14] fabricated an automatic photocatalytic reactor using a bundle of five unidimensional capillaries together (Fig. 3). The capillary dimensions were 1.1 mm internal diameter, 1.3 mm outer diameter and 6 cm in length,

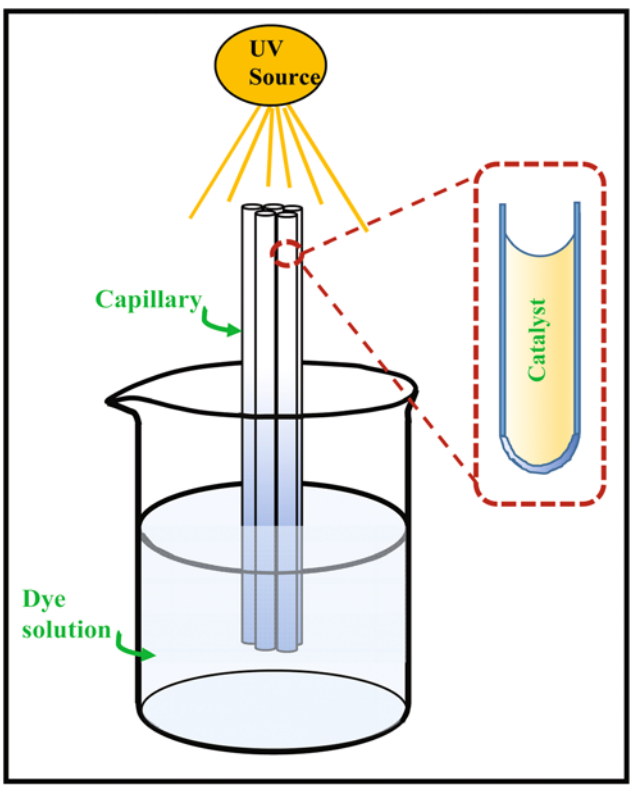


Fig. 3 Schematic of the experimental set up of a capillary microreactor used by Katayama *et al.*[14]

and the inside was coated with tungsten oxide. The capillary bundle was kept in an optical cell occupied with dye solution, and the reactant solution goes inside the capillary due to the capillary force under quasi-sunlight exposure. The dye degradation was up to ~91% after a few hours of exposure. Maximum dye degradation was observed within an optimal

diameter 0.9–1.2 mm, which shows that a smaller diameter gives a better result than a larger diameter.

**4.2.3. Silica capsule.** Yamada *et al.*[121] encapsulated the $TiO_2$ nanoparticles within hollow mesoporous silica capsules to fabricate a microreactor. The monodispersed mesoporous silica spheres were synthesized by using amino-modified polystyrene beads as a template. The microreactor evaluated the photocatalytic activity of methyl orange and methylene blue. The photocatalytic activity of the $TiO_2$-encapsulated microreactor displayed higher degradation efficiency towards methyl orange, especially at the initial stage of the reaction.

**4.2.4. Quartz.** Matsushita *et al.*[122] fabricated a quartz microreactor with a straight microchannel of 500 μm width, 10–500 μm depth, and 50 mm length using a micromilling process for the photodegradation of organic pollutants such as chlorophenol, bisphenol A, and dimethylformamide (DMF) under UV-LED irradiation. The sol–gel process was used to coat the bottom and side walls of the microchannel with a photocatalytic $TiO_2$ layer. The results showed higher dye degradation within a few seconds.

### 4.3 Metallic microreactor

**4.3.1. Titanium.** Krivec *et al.*[123] fabricated a $TiO_2$-based microreactor on a titanium foil using a high-precision computer numerical control (CNC) milling machine. A serpentine microchannel with cross-sectional dimensions of approximately 500 μm × 500 μm and a length of 390 mm was engraved. Afterwards, by anodic oxidation and a hydrothermal method, the titanium surface of the microchannel inner walls was coated with a mixture of $TiO_2$ nanotubes and nanoparticles. $TiO_2$-coated titanium foil was sealed with UV-transparent plexiglass by epoxy glue and four 0.8 mW UV LEDs combined with a power controller on a small printed-circuit board were fixed over the substrate. Two holes of 2 mm were made on the plexiglass surface for the inlet and outlet system. Caffeine was taken as a model degradation molecule which was pumped within the microchannel by a high-precision syringe pump. The results showed very high photocatalytic efficiency and after 6 months of use and 3600 working cycles, the microreactor still exhibited 60% of its initial efficiency.

**4.3.2. Stainless steel.** Eskandarloo *et al.*[124] designed an array of microchannels with dimensions of about 400 μm width, 50 μm depth, and 54 cm length on a flat stainless steel plate using a $CO_2$ laser technique. Within a 2 cm length, the microchannel turned 30 times. The sol–gel method was used to synthesize $TiO_2$ nanoparticles on the inner wall of the microchannels by pumping titanium *n*-butoxide/ethanol and water into the microchannels. A silver nitrate solution was pumped into the $TiO_2$ catalyst bed microchannels in the presence of UV-LED irradiation to prepare the $Ag/TiO_2$ microreactor. Terephthalic acid was used as a model organic pollutant to determine the photocatalytic efficiency of the $Ag/TiO_2$ microreactor under UV-LED irradiation. The Ag (0.8 wt%)/$TiO_2$ catalyst bed microreactor showed higher photocatalytic efficiency than pure $TiO_2$, $Ag/TiO_2$ catalyst bed and $TiO_2$-P25 catalyst. At optimum conditions (10.22 μl $min^{-1}$ flow rate, 12.94 mg $L^{-1}$ inlet concentration, 6.2 initial solution pH, and 7.53 $Wm^{-2}$ min UV-LEDs light intensity), a maximum removal efficiency of 98.8% was observed.

**4.3.3. Aluminum oxide.** Aran *et al.*[125] demonstrated a new membrane microreactor concept for multiphase photocatalytic reactions which included five steps, such as porous α-$Al_2O_3$ substrate fabrication, microfabrication, photocatalyst immobilization, surface modification and module assembly, to develop a porous photocatalytic membrane microreactor (P2M2). The results of photocatalytic degradations of MB and phenol showed enhanced degradation efficiency.

### 4.4 Ceramic microreactor

**4.4.1. Porous alumina ceramic disks.** A $TiO_2$-coated porous ceramic microchannel reactor was designed by Teekateerawej *et al.*[126,127] for the photocatalytic degradation of MB dye solution. As a base material for photocatalytic microchannel fabrication, porous alumina ceramic disks of diameter 5.0 mm, and thickness 0.2 mm, containing 1250 channels of 50 μm diameter in a 3.0 mm circle, were used. A pyrolysis method was used to prepare a $TiO_2$ layer inside the ceramic channel surface using TA/PVP solution and commercial grade titania sol (Mitsubishi Gas Chemical). Irrespective of flow rate, the titania sol based microreactor showed higher photocatalytic activity than that prepared from TA/PVP solution. Analysis showed that the channel surface profile is an important parameter, because the roughness of the $TiO_2$ surface creates a stagnation region which retards the mass transfer from the channel wall to the laminar region of the channel flow.

**4.4.2. Low temperature co-firing ceramic.** Gorges *et al.*[128] manufactured a $TiO_2$ catalyst coated photocatalytic microreactor using a high-precision CNC milling machine. 19 microchannels with a cross-section of ≈300 μm × 200 μm were milled. The microstructure with an immobilized $TiO_2$ catalyst was sealed with a glass top using epoxy glue and mounted in stainless steel housing. 4-Chlorophenol was used as a model substrate for degradation. A maximum of 40% degradation was observed at a flow rate of 3 μl $m^{-1}$. The reactions' intrinsic kinetic parameters were calculated and mass-transfer limitations for reaction operating conditions could be excluded by calculating appropriate Damköhler numbers.

A summary of all the above-discussed microchannel fabrication techniques, materials used, catalysts used, and source of light is provided in Table 1.

## 5. Factors effecting the photocatalytic degradation within microchannel

In a microreactor, the dye degradation efficiency is effected by a few important parameters, such as the flow rate, initial concentration of the target compound ($C_o$), microreactor dimensions, and light intensity, which are all discussed below.

 

Table 1 Summary of utilization of microchannel for photocatalytic degradation

| Fabrication technique | Materials | Dye degraded | Catalyst used | Source of light | References |
|---|---|---|---|---|---|
| Soft lithography | PDMS | Methylene blue | $TiO_2$ | UV | Meng *et al.*[19] |
| Casting and replicate technology | PDMS | Methylene blue | $TiO_2$ | UV | Lamberti *et al.*[106] |
| Soft lithography | PDMS | Methylene blue | ZnO | UV | Han *et al.*[107] |
| Soft lithography | PDMS | Methylene blue | $TiO_2$ | UV | Rasponi *et al.*[108] |
| $CO_2$ laser technique | PMMA | Textile dyes such as acid orange 7, acid violet 19, methyl orange, and malachite green | $TiO_2$ | UV-LED | Eskandarloo and Badiei[109] |
| Molding technology | PDMS, gel | Methylene blue | $TiO_2$ | UV | Koo and Velev[110] |
| Microcapillary | Silica | Coccine, sunset yellow, methyl red, rhodamine 6G, erythrosine and methylene blue | $TiO_2$ | UV | Tsuchiya *et al.*[3] |
| Commercial | Glass | Methyl orange | $TiO_2$ | UV | Shen *et al.*[15] |
| Commercial | Glass | Phenol | Pt/ZnO | | Zhang *et al.*[16] |
| Commercial | — | Rhodamine 6G | $TiO_2$ | UV | Oda *et al.*[120] |
| Stereolithography | Epoxy resin | Salicylic acid | $TiO_2$ | UV | Charles *et al.*[111] |
| Stereolithography | Epoxy resin | Salicylic acid | $TiO_2$ | (UV-A) light | Corbel *et al.*[112] |
| Commercial | Glass | Methylene blue | $TiO_2$/ZnO | UV | He *et al.*[117] |
| UV lithography | Glasses | Methylene blue | $TiO_2$ | UV | Lei *et al.*[114] |
| Self-assembly technique | Silica glass | Methylene blue | $SiO_2$/$TiO_2$ | UV | Li *et al.*[118] |
| Direct write laser lithography | Soda-lime glass blank wafers | Methylene blue | $TiO_2$ | UV-LED | Lindstrom *et al.*[115] |
| UV imprinting lithography | Glass | 4-Chlrophenol | $TiO_2$ | | Yoon *et al.*[113] |
| Synthetic method | Silica | Methyl orange and methylene blue | $TiO_2$ | | Yamada *et al.*[121] |
| Commercial | Glass | Methylene blue | $TiO_2$ | UV-LED | Ramos *et al.*[116] |
| Micromilling | Quartz | Chlorophenols, bisphenol A, and dimethylformamide | $TiO_2$ | UV-LED | Matsushita *et al.*[122] |
| — | Silica-glass capillary | Methylene blue | $TiO_2$, $SiO_2$/$TiO_2$ | UV-lamp | Nakamura *et al.*[119] |
| High-precision computer numerical control (CNC) milling machine | Metal–titanium foil | Caffeine | $TiO_2$ | UV-LED irradiation | Krivec *et al.*[123] |
| $CO_2$ laser technique | Flat stainless steel plate | Terephthalic acid | $TiO_2$ | UV-LED irradiation | Eskandarloo *et al.*[124] |
| New membrane microreactor concept | Porous α-$Al_2O_3$ | Methylene blue and phenol | $TiO_2$ | UV | Aran *et al.*[125] |
| Commercial | Ceramic | Methylene blue | $TiO_2$ | UV | Teekateerawej *et al.*[126,127] |
| High-precision CNC milling machine | Ceramic | 4-Chlorophenol | $TiO_2$ | UV-A | Gorges *et al.*[128] |

### 5.1 Flow rate

It has been demonstrated that the flow rate of the dye solution is an important parameter for dye degradation within microchannels. Fig. 4(a) shows a plot of degradation efficiency *versus* flow rate using experimental data extracted from various previous studies. In some studies where the flow rate was not mentioned, it was calculated from the data reported (residence time) in the corresponding papers. From Fig. 4(a), it is observed that the dye degradation efficiency decreases sharply with an increase in flow rate. For example, Meng *et al.*[19] showed that with a decrease in flow rate from 100 μl $min^{-1}$ to 25 μl $min^{-1}$ (a corresponding residence time increase from 12.43 s to 53.00 s), MB degradation increased sharply and completely degraded occurred in less than 1 min. Aran *et al.*[125] studied the MB degradation for different liquid flow rates: 10, 30 and 50 μl $min^{-1}$ (residence times: 3.3, 0.7 and 0.3 min, respectively) and observed the same trend, with the MB degradation efficiencies being 90%, 55% and 35%, respectively. Eskandarloo and Badiei[109] also studied the influence of the flow rate on the performance of a photocatalytic micro-photoreactor. Analysis showed that the degradation efficiency of 4-NP increased from 76% to 100% with a decrease in the flow rate from 150 to 10 μl $min^{-1}$ (corresponding residence times of 6.4 and 96 s), respectively. Eskandarloo *et al.*[124] and Corbel *et al.*[129] also observed a similar trend of degradation efficiency with flow rate. Other researchers, like Choi *et al.*,[130] Lei *et al.*[114] and Gao *et al.*[131] have shown similar trends of degradation with a very wide range of flow rates from 0 to 10 ml $min^{-1}$. The phenomenon of increasing degradation efficiencies with a decrease in flow rate is due to the increase in residence time of the reactant solution inside the microchannels.

### 5.2 Initial dye concentration ($C_o$)

In general, for a batch reactor, research shows that with increasing $C_o$, the degradation rate increases to an extent, and a further increase in $C_o$ leads to a decrease in degradation rate.[132,133] However, in microchannels, it has been generally observed that the dye degradation efficiency decreases with an

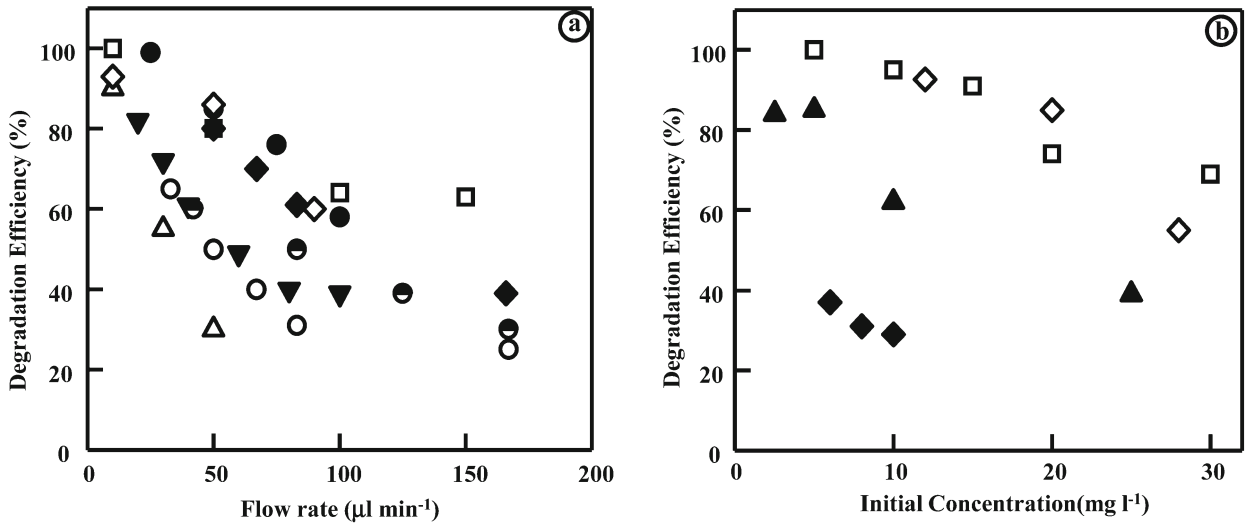


Fig. 4 Photocatalytic degradation efficiency as a function of (a) flow rate and (b) initial dye concentration. The circle, triangle, rectangle, rhombus, filled rhombus, filled triangle, filled circle and half-filled circle symbols represent Meng *et al.*,[19] Aran *et al.*,[125] Eskandarloo *et al.*,[109] Eskandarloo *et al.*,[124] Charles *et al.*,[111] Krivec *et al.*,[123] Corbel *et al.*[112] and Corbel *et al.*,[129] respectively.

increase in $C_o$. The degradation efficiency as a function of initial dye concentration is shown in Fig. 4(b), where data are extracted from previously reported studies.[108,110,122,123] A possible explanation for this phenomena of degradation rate depends on the probability of $^{\bullet}OH$ radical formation at the catalyst surface and $^{\bullet}OH$ radicals reacting with dye molecules. A higher $C_o$ requires more reactive radical species for the reaction. Within microchannels, a fixed amount of reactive radical species form under fixed experimental conditions such as flow rate, microchannel length, and light intensity. Furthermore, with an increase in $C_o$, organic substances and intermediates molecules get adsorbed on the immobilized catalyst surface which reduces the degradation efficiency due to the decrease in the production of reactive radical species like $^{\bullet}OH$ and $O_2^{-\bullet}$.[134–136]

### 5.3 Initial pH of solution

The initial pH of the solution shows a significant effect on dye degradation. Eskandarloo *et al.*[124] showed that by increasing the initial solution pH from 4 to 6, the removal rate increased from 65.23% to about to 85.8%. Upon further increase in pH, the degradation decreased to 40.02%. Similarly, Gao *et al.*[131] also showed that with an increase of the initial pH of the dye solution from 2 to 9, the decolorization efficiency increased from 64% to 87%, and with a further increase in initial pH from 9 to 12, a decrease in decolorization efficiency from 87% to 82% was shown. At lower pH values, the reactive positive holes are major oxidation species whereas at neutral or high pH levels, hydroxyl radicals act as the predominant species. The formation of hydroxyl radicals, by oxidizing hydroxide ions available on the $TiO_2$ surface, is easier in alkaline conditions than in acidic conditions, which initially enhances the degradation efficiency. After a certain pH value, there is a Coulombic repulsion between the negatively charged surface of the photocatalyst and the hydroxide anions. Also, at a higher pH, the concentration of hydroxyl radicals is greater than the ozone concentration, which causes the reaction between the same radicals to predominate over the reaction among radicals and dye molecules, thus reducing the dye degradation.[137–141]

### 5.4 Microreactor dimension

The length of the microreactor has a significant effect on the degradation efficiency of dyes. Charles *et al.*[111] showed that the degradation efficiency could be increased along with the length of the microchannel for a small range of lengths from 20 to 70 mm. Eskandarloo and Badiei[109] also reported a similar kind of phenomena of degradation efficiency for a wide range of microchannel lengths. This study showed that the degradation efficiency was increased from 19 to 70% by increasing the length from 10 to 70 cm. With increasing microchannel length, the residence time of the dye within the microreactor increases. Therefore, the contact time between the dye molecule and immobilized catalyst increases, which enhances the photocatalytic reaction.[142] The inner diameter of the microchannel also has a significant effect on the performance of dye degradation. Nakamura *et al.*[119] demonstrated that a smaller diameter microchannel shows better performance in the degradation of methylene blue dye. With a decreasing channel diameter, a greater number of dye molecules react with the catalyst, which enhances the initial reaction rate.

### 5.5 Light intensity

The light intensity has an important effect on the photocatalytic degradation rate. Fig. 5(a) shows the degradation profile with respect to light intensity, where data are extracted from previously reported studies.[109,111,124] The degradation of organic compounds gets enhanced with an increase in incident UV light intensity. During the photocatalytic reaction,

 

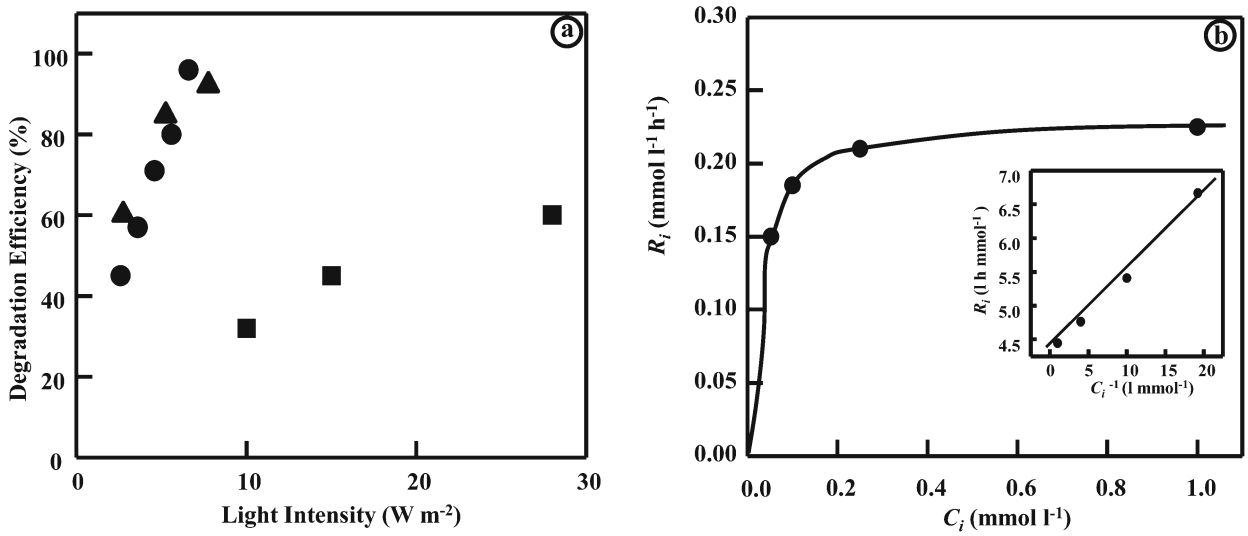


Fig. 5 (a) Photocatalytic degradation efficiency of a microreactor with light intensity, where circle, triangle and rectangle symbols represent Eskandarloo *et al.*,[109] Eskandarloo *et al.*[124] and Charles *et al.*,[111] respectively. (b) Reaction rate with respect to initial pollutant concentration, Gorges *et al.*[128]

photons produced by light irradiation transfer the electron from the valence band of the catalyst to the conduction band, which further decomposes the organic compound as per eqn (1)–(6). Therefore, the degradation rate depends on photon production, *i.e.*, in other words, on light irradiation. At lower light intensity, electron–hole formations are predominant and electron–hole recombination is negligible, which decreases the formation rate of hydroxyl radicals. Under more intense radiation, more hydroxyl radicals are generated, increasing the removal rate.[143–146]

### 5.6 Catalyst structure

Fine-tuning of the physical morphology, such as adjusting the size or structure of semiconductors helps in achieving enhanced photocatalytic properties. It is known that higher crystallinity reduces the numbers of defects on the catalyst surface or in the bulk, which reduces the possibility of recombination of electrons and holes. A higher calcination temperature improves the crystallinity, however, it decreases the porosity. Thus, experimental conditions should be carefully optimized to get the highest activity.[147] Charge recombination rates can be decreased and the photocatalytic activity can be improved by decreasing the particle size to the nanoscale, at which the bulk diffusion length of the charge carriers gets shortened.[147] According to structural characteristics, photocatalytic materials are classified as zero-/two-dimensional, one dimensional and multi-dimensional materials.[148] Solid membranes, films and powders are zero-dimensional photocatalytic materials, which can be fabricated using facile methods. These materials have a quantum confinement effect if synthesized and used at the nanoscale, and they strongly influence the position of conduction and valence bands.[149–151] A small size shifts the conduction band to a more negative value due to size-quantization effects. Ultrathin nanoplates help the charge carriers to move rapidly from the interior to the surface, thus improving the separation of the photogenerated electron and hole, and hence, improving the photocatalytic activity. However, small particles tend to aggregate due to their larger surface energy. Surfactants are used to stabilize the small particles. Also, small particles are difficult to recycle after the photocatalytic process. Photocatalytic films overcome this drawback.[147] Nanorods, nanoparticles, nanowires (NWs), *etc*. fall under the category of one dimensional photocatalytic materials. These materials may be hollow and porous and thus supplement the surface area and allow easy organic material diffusion. In addition, these have high electron transport efficiency.[152–156] Hierarchical assemblies that combine the two- or three-dimensional structures are called multi-dimensional materials. These materials have further augmented surface area and show structure-induced characteristics, such as multiple reflections of incident light, inner trapping of pollutants, *etc*.[148] Hierarchical structured photocatalysts also enhance light absorption, enhance electron transport along the nanoplates and facilitate electrolyte diffusion due to their open structure.[147]

### 5.7 Catalyst support

The catalytic activity of photocatalysts can be enhanced by the proper selection of supports with a high surface area. Heterogeneous photocatalyst supports enhance the photocatalytic activity due to the synergistic interaction between the photocatalyst and the support. Supports enhance the charge separation and thus provide better electric conductivity. High porous area supports adsorb the organic molecule to be degraded and easily desorb the degradation products.[157] Degradation of the adsorbed organic molecules becomes more

Table 2 Kinetic parameter values from the literature

| References | Reaction rate constant, $k_s$ (mmol $l^{-1}$ $h^{-1}$) | Adsorption coefficient, $K$, (l $mmol^{-1}$) |
|---|---|---|
| Krivec *et al.*[123] | 1.82 | 17 |
| Choi *et al.*[130] | 0.75 | 22 |
| Charles *et al.*[111] | $1.7 \times 10^{-3}$ (mmol $l^{-1}$ $S^{-1}$) | 24 |
| Gorges *et al.*[128] | 0.26 | 28 |
| Theurich *et al.*[163] | 0.2 | 24 |

likely because of its increased and easy interactions with the hydroxyl radical which is available on the catalyst support itself.[147,158] Dispersion of the photocatalyst on a support helps in its proper dispersion and prevents its agglomeration and sintering.[159,160] Supports immobilize the photocatalysts and thus increase its reusability.[161,162]

## 6. Kinetic study of photocatalytic degradation within microreactors

Some studies been reported on the kinetics of photocatalytic degradation within microchannels by Krivec *et al.*,[123] Choi *et al.*,[130] Gorges *et al.*[128] and Charles *et al.*[111] In general, a microfludic reactor has been considered to be a perfect plug-flow reactor and the photocatalytic degradation is often described by the Langmuir–Hinshelwood kinetics model. The degradation reaction rate has been represented by the following equation:

$$R_i = \frac{k_s K C_i}{1 + K C_i}, \quad (7)$$

where $R_i$ and $k_s$ denote the reaction rate of compound degradation and the reaction rate constant, respectively. $C_i$ and $K$ signify the initial pollutant concentration and the adsorption coefficient of pollutant substrate on the photocatalyst surface, respectively. The linearization of eqn (7) results in a linear relationship with an intercept of ${k_s}^{-1}$ and a slope of $(k_s K)^{-1}$:

$$\frac{1}{R_i} = \frac{1}{k_s} + \frac{1}{k_s K}\frac{1}{C_i} \quad (8)$$

The reaction rate constant and adsorption coefficient are calculated using eqn (7) and (8) as shown in Fig. 5(b) and Table 2. The reaction rate constant is strongly dependent upon experimental conditions; therefore, it is not possible to compare the $k_s$ values determined by different researchers. However, variation in the values of adsorption coefficient is marginal.[111,128,163]

## 7. Summary and future perspectives

The fabrication and usage of microreactors for photochemical applications is still in the research stage and has not been commercialized yet as an industrial process. This is because of the high cost of fabrication and immobilization of costlier catalysts. There are many challenges which need to be addressed with respect to the presence of catalysts inside a microreactor, like the method of fixation of catalyst inside the microreactor, retaining the catalyst and its activity for longer duration, removing the spent catalyst and avoiding plugging of the microreactor. In addition to the above, there are greater challenges with respect to the removal of various mass-transfer resistances. Moreover, studies on comparisons of capital and operating costs of the microreactor with respect to conventional reactors are very scarce. Microreactors or microchannel fabrication of different materials with precise dimensions are still a big challenge. Microchannels are easier to make on metallic substrates as compared to polymeric substrates, however, the reactive and opaque nature of metallic substrates make them non-preferred substrates for making microreactors for photochemical applications. Polymeric substances have problems with respect to their brittle nature, which causes fractures inside the microreactors. Other materials are costlier and have problems with absorption of heat. Conventional fabrication techniques such as lithography and etching are time consuming and have shortcomings with respect to the manufacture of precise and wide-dimensional microreactors. In the embossing and imprinting techniques, wearing of the stamp, which incorporates features of the microreactors, results in improper dimensions. Laser fabrication technique is more efficient, less time-consuming and seems to be a more prospective technique, although damages due to its inherent thermal nature still need to be addressed. Microreactors can do the same to microchemical reactor engineering what transistors did to microelectronics. To do this, their throughput has to be increased. This can be done by two approaches: one in which the parallelization of microreactors has to be done; and in the other, increasing the microreactor dimensions and flow rates. The second approach has likely chances of losing the advantages of better mass and heat transfer rates in microreactors. For use of the first method, microreactors have to be integrated with sensors, controllers and actuators through lab-on-chip techniques and/or through integrated hybrid schemes. In addition, accurate and complex control systems have to be developed so that all units have identical operating conditions. The packaging of several microreactors into a bigger unit is also a significant challenge.

This article gives an overview of photocatalytic microreactors with an application in environmental science, in particular, the degradation of different toxic dyes within microchannels. Various microreactor fabrication techniques, depending on the application, have been demonstrated. This paper also gives an idea about the effect of parameters such as flow rate, initial dye concentration, initial pH of solution, microreactor dimensions and light intensity on dye degradation efficiency within microreactors, including kinetic studies. Taking advantage of the enhanced heat and mass transfer within microchannels, the photocatalytic dye degradation performance will be higher in a microreactor than a batch reactor; however, a lot of challenges lie ahead before its commercial and industrial usage.

## References


1 T. V. Gerven, G. Mul, J. Moulijn and A. Stankiewicz, A Review of Intensification of Photocatalytic Processes, *Chem. Eng. Process.*, 2007, **46**, 781–789.

2 M. E. Leblebici, G. D. Stefanidis and T. V. Gerven, Comparison of Photocatalytic Space-time Yields of 12 Reactor Designs for Wastewater Treatment, *Chem. Eng. Process.*, 2015, **97**, 106–111.

3 N. Tsuchiya, K. Kuwabara, A. Hidaka, K. Oda and K. Katayama, Reaction Kinetics of Dye Decomposition Processes Monitored inside a Photocatalytic Microreactor, *Phys. Chem. Chem. Phys.*, 2012, **14**, 4734–4741.

4 Priyanka and V. C. Srivastava, Photocatalytic Oxidation of Dye Bearing Wastewater by Iron Doped Zinc Oxide, *Ind. Eng. Chem. Res.*, 2013, **52**, 17790–17799.

5 P. R. Potti and V. C. Srivastava, Comparative Studies on Structural, Optical, and Textural Properties of Combustion Derived ZnO Prepared Using Various Fuels and Their Photocatalytic Activity, *Ind. Eng. Chem. Res.*, 2012, **51**, 7948–7956.

6 A. Mills and J. Wang, Photomineralisation of 4-chlorophenol Sensitised by $TiO_2$ Thin Films, *J. Photochem. Photobiol., A*, 1998, **118**, 53–63.

7 M. F. J. Dijkstra, H. J. Panneman, J. G. M. Winkelman, J. J. Kelly and A. A. C. M. Beenackers, Modeling the Photocatalytic Degradation of Formic Acid in a Reactor with Immobilized Catalyst, *Chem. Eng. Sci.*, 2002, **57**, 4895–4907.

8 T. Oyama, A. Aoshima, S. Horikoshi, H. Hidaka, J. Zhao and N. Serpone, Solar Photocatalysis, Photodegradation of a Commercial Detergent in Aqueous $TiO_2$ Dispersions under Sunlight Irradiation, *Solar Energy*, 2004, **77**, 525–532.

9 D. Robert and S. Malato, Solar Photocatalysis: A Clean Process for Water Detoxification, *Sci. Total Environ.*, 2002, **291**, 85–97.

10 S. Malato, J. Blanco, A. Vidal, D. Alarcon, M. I. Maldonado, J. Caceres and W. Gernjak, Applied Studied in Solar Photocatalytic Detoxification: An Overview, *Solar Energy*, 2003, **75**, 329–336.

11 H. Lu, M. A. Schmidt and K. F. Jensen, Photochemical Reactions and On-line UV Detection in Microfabricated Reactors, *Lab Chip*, 2001, **1**, 22–28.

12 R. C. R. Wootton, R. Fortt and A. J. de Mello, A Microfabricated Nanoreactor for Safe, Continuous Generation and Use of Single Oxygen, *Org. Process Res. Dev.*, 2002, **6**, 187–189.

13 H. Ehrich, D. Linke, K. Morgenschweis, M. Baerns and K. Jahnisch, Application of Microstructured Reactor Technology for the Photochemical Chlorination of Alkylaromatics, *Chimia*, 2002, **56**, 647–653.

14 K. Katayama, Y. Takeda, K. Kuwabara and S. Kuwahara, A Novel Photocatalytic Microreactor Bundle that does not Require an Electric Power Source, *Chem. Commun.*, 2012, **48**, 7368–7370.

15 C. Shen, Y. J. Wang, J. H. Xu and G. S. Luo, Glass Capillaries with $TiO_2$ Supported on Inner Wall as Microchannel Reactors, *Chem. Eng. J.*, 2015, **277**, 48–55.

16 Q. Zhang, Q. Zhang, H. Wang and Y. Li, A High Efficiency Microreactor with Pt/ZnO Nanorod Arrays on the Inner Wall for Photodegradation of Phenol, *J. Hazard. Mater.*, 2013, **254–255**, 318–324.

17 J. Parmar, S. Jang, L. Soler, D. Kim and S. Sanchez, Nanophotocatalysts in Microfluidics, Energy Conversion and Environmental Applications, *Lab Chip*, 2015, **15**, 2352–2356.

18 S. S. Ahsan, A. Gumus and D. Erickson, Redox Mediated Photocatalytic Water-Splitting in Optofluidic Microreactors, *Lab Chip*, 2013, **13**, 409–414.

19 Z. Meng, X. Zhanga and J. Qin, A High Efficiency Microfluidic-Based Photocatalytic Microreactor Using Electrospun Nanofibrous $TiO_2$ as a Photocatalyst, *Nanoscale*, 2013, **5**, 4687–4690.

20 L. Schneegass, R. Bräutigam and J. M. Köhler, Miniaturized Flow-through PCR with Different Template Types in a Silicon Chip Thermocycler, *Lab Chip*, 2001, **1**, 42–49.

21 Y. Kikutani, T. Horiuchi, K. Uchiyama, H. Hisamoto, M. Tokeshi and T. Kitamori, Glass Microchip with Three-Dimensional Microchannel Network for 2 × 2 Parallel Synthesis, *Lab Chip*, 2002, **2**, 188–192.

22 Y. Cheng, K. Sugioka and K. Midorikawa, Microfabrication of 3D Hollow Structures Embedded in Glass by Femtosecond Laser for Lab-on-a-Chip Applications, *Appl. Surf. Sci.*, 2005, **248**, 172–176.

23 O. Hofmann, P. Niedermann and A. Manz, Modular Approach to Fabrication of Three-dimensional Microchannel Systems in PDMS Application to Sheath Flow Microchips, *Lab Chip*, 2001, **1**, 108–114.

24 M. Svedberg, M. Veszelei, J. Axelsson, M. Vangbo and F. Nikolajeff, Poly (dimethylsiloxane) Microchip: Microchannel with Integrated Open Electrospray Tip, *Lab Chip*, 2004, **4**, 322–327.

25 L. H. Hung, R. Lin and A. P. Lee, Rapid Microfabrication of Solvent-Resistant Biocompatible Microfluidic Devices, *Lab Chip*, 2008, **8**, 983–987.

26 M. Natali, S. Begolo, T. Carofiglioc and G. Mistura, Rapid Prototyping of Multilayer Thiolene Microfluidic Chips by Photopolymerization and Transfer Lamination, *Lab Chip*, 2008, **8**, 492–494.

27 H. B. Yu, G. Y. Zhou, F. K. Chau and F. W. Lee, Optoluidic Variable Aperture, *Opt. Lett.*, 2008, **33**, 548–550.

28 C. L. Bliss, J. N. McMullin and C. J. Backhouse, Rapid Fabrication of A Microfluidic Device with Integrated Optical Waveguides for DNA Fragment Analysis, *Lab Chip*, 2007, **7**, 1280–1287.

29 I. K. Konstantinou and T. A. Albanis, Photocatalytic Transformation of Pesticides in Aqueous Titanium Oxide Suspensions Using Artificial and Solar Light: Intermediates and Degradation Pathways, *Appl. Catal., B*, 2003, **42**, 319–335.

30 J. M. Hermann, Heterogeneous Photocatalysis: Fundamentals and Applications to the Removal of Various Types of Aqueous Pollutants, *Catal. Today*, 1999, **53**, 115–129.

31 H. D. Burrows, M. Canle, J. A. Santaballa and S. Steenken, Reaction Pathways and Mechanisms of Photodegradation of Pesticides, *J. Photochem. Photobiol., B*, 2002, **67**, 71–108.

32 S. Chiron, A. Fernández-Alba, A. Rodriguez and E. C. Calvo, Pesticide Chemical Oxidation: State of the Art, *Water Res.*, 2000, **34**, 366–377.

33 V. K. Gupta, R. Jain, A. Mittal, T. A. Saleh, A. Nayak, S. Agarwal and S. Sikarwar, Photo-catalytic Degradation of Toxic Dye Amaranth on $TiO_2$/UV in Aqueous Suspensions, *Mater. Sci. Eng., C*, 2012, **32**, 12–17.

34 H. Eskandarloo, A. Badiei, M. A. Behnajady and G. M. Ziarani, Minimization of Electrical Energy Consumption in the Photocatalytic Reduction of Cr(VI) by Using Immobilized Mg, Ag, Co-impregnated $TiO_2$ Nanoparticles, *RSC Adv.*, 2014, **4**, 28587–28596.

35 M. A. Behnajady and H. Eskandarloo, Silver and Copper Co-impregnated onto $TiO_2$–$P_{25}$ Nanoparticles and its Photocatalytic Activity, *Chem. Eng. J.*, 2013, **228**, 1207–1213.

36 M. A. Behnajady and H. Eskandarloo, Characterization and Photocatalytic Activity of Ag–Cu/$TiO_2$ Nanoparticles Prepared by Sol-gel Method, *J. Nanosci. Nanotechnol.*, 2013, **13**, 548–553.

37 J. Saien and S. Khezrianjoo, Degradation of the Fungicide Carbendazim in Aqueous Solutions with UV/$TiO_2$ Process: Optimization, Kinetics and Toxicity Studies, *J. Hazard. Mater.*, 2008, **157**, 269–276.

38 V. K. Gupta, R. Jain, A. Mittal, M. Mathur and S. Sikarwar, Photochemical Degradation of the Hazardous Dye Safranin-T Using $TiO_2$ Catalyst, *J. Colloid Interface Sci.*, 2007, **309**, 464–469.

39 J. Schwitzgebel, J. G. Ekerdt, H. Gerischer and A. Heller, Role of the Oxygen Molecule and of the Photogenerated Electron in $TiO_2$-photocatalyzed Air Oxidation Reactions, *J. Phys. Chem.*, 1995, **99**, 5633–5638.

40 S. Xiong, S. George, Z. Ji, S. Lin, H. Yu, R. Damoiseaux, B. France, K. W. Ng and S. C. J. Loo, Size of $TiO_2$ Nanoparticles Influences Their Phototoxicity: An in Vitro Investigation, *Arch. Toxicol.*, 2013, **87**, 99–109.

41 A. Fujishima, X. Zhang and D. A. Tryk, $TiO_2$ Photocatalysis and Related Surface Phenomena, *Surf. Sci. Rep.*, 2008, **63**, 515–582.

42 M. Ni, M. K. H. Leung, D. Y. C. Leung and K. Sumathy, A Review and Recent Developments in Photocatalytic Water-Splitting Using $TiO_2$ for Hydrogen Production, *Renewable Sustainable Energy Rev.*, 2007, **11**, 401–425.

43 Y. Yu, J. C. Yu, J. G. Yu, Y. C. Kwok, Y. K. Che, J. C. Zhao, L. Ding, W. K. Ge and P. K. Wong, Enhancement of Photocatalytic Activity of Mesoporous $TiO_2$ by Using Carbon Nanotubes, *Appl. Catal., A*, 2005, **289**, 186–196.

44 M. N. Chong, B. Jin, C. W. K. Chow and C. Saint, Recent Developments in Photocatalytic Water Treatment Technology: A Review, *Water Res.*, 2010, **44**, 2997–3027.

45 M. Pelaez, N. T. Nolan, S. C. Pillai, M. K. Seery, P. Falaras, A. G. Kontos, P. S. M. Dunlop, J. W. J. Hamilton, J. A. Byrne, K. O'Shea, M. H. Entezari and D. D. Dionysiou, A Review on the Visible Light Active Titanium Dioxide Photocatalysts for Environmental Applications, *Appl. Catal., B*, 2012, **125**, 331–349.

46 J. C. Yu, J. Yu, W. Ho, Z. Jiang and L. Zhang, Effects of F-Doping on the Photocatalytic Activity and Microstructures of Nanocrystalline TiO2 Powders, *Chem. Mater.*, 2002, **14**, 3808–3816.

47 H. Wang and J. P. Lewis, Effects of Dopant States on Photoactivity in Carbon-Doped $TiO_2$, *J. Phys.: Condens. Matter*, 2005, **17**, L209–L213.

48 J. Ananpattarachai, P. Kajitvichyanukul and S. Seraphin, Visible Light Absorption Ability and Photocatalytic Oxidation Activity of Various Interstitial N-doped $TiO_2$ Prepared from Different Nitrogen Dopants, *J. Hazard. Mater.*, 2009, **168**, 253–261.

49 M. Ghaffari, H. Huang, P. Y. Tan and O. K. Tan, Synthesis and Visible Light Photocatalytic Properties of $SrTi(1-x)Fe_xO(3-\sigma)$ Powder for Indoor Decontamination, *Powder Technol.*, 2012, **225**, 221–226.

50 S. Sakthivel and H. Kisch, Daylight Photocatalysis by Carbonmodified Titanium Dioxide, *Angew. Chem., Int. Ed.*, 2003, **42**, 4908–4911.

51 T. Morikawa, R. Asahi, T. Ohwaki, K. Aoki, K. Suzuki and Y. Taga, Visible-Light Photocatalyst-Nitrogen Doped Titanium Dioxide, *R&D Rev. Toyota CRDL*, 2005, **40**, 45–50.

52 N. Sobana, M. V. Muruganandam and M. S. Swaminathan, Characterization of AC–ZnO Catalyst and its Photocatalytic Activity on 4-acetylphenol Degradation, *Catal. Commun.*, 2008, **9**, 262–268.

53 Y. Wu, M. Xing, B. Tian, J. Zhang and F. Chen, Preparation of Nitrogen and Fluorine Co-Doped Mesoporous $TiO_2$ Microsphere and Photodegradation of Acid Orange 7 under Visible Light, *Chem. Eng. J.*, 2010, **162**, 710–717.

54 T. Yu, X. Tan, L. Zhao, Y. Yin, P. Chen and J. Wei, Characterization, Activity And Kinetics of A Visible Light Driven Photocatalyst: Cerium and Nitrogen Co-Doped $TiO_2$ Nanoparticles, *Chem. Eng. J.*, 2010, **157**, 86–92.

55 N. Bao, Q. Zhang and J.-J. Xu, Fabrication of Poly (dimethylsiloxane) Microfluidic System Based on Masters Directly Printed with an Office Laser Printer, *J. Chromatogr., A*, 2005, **1089**, 270–275.

56 A. Muck, J. Wang and M. Jacobs, Fabrication of Poly (methyl methacrylate) Microfluidic Chips by Atmospheric Molding, *Anal. Chem.*, 2004, **76**, 2290–2297.

57 S. L. R. Barker, M. J. Tarlov and H. Canavan, Plastic Microfluidic Devices Modified with Polyelectrolyte Multilayers, *Anal. Chem.*, 2000, **72**, 4899–4903.

58 X. Bai, C. Roussel and H. Jensen, Polyelectrolyte-Modified Short Microchannel for Cation Separation, *Electrophoresis*, 2004, **25**, 931–935.

59 S. J. Qin and W. J. Li, Micromachining of Complex Channel Systems in 3D Quartz Substrates Using Q-Switched Nd: YAG Laser, *Appl. Phys. A: Mater. Sci. Process.*, 2002, **74**, 773–777.

60 P. Pal and K. Sato, Various Shapes of Silicon Freestanding Microfluidic Channels and Microstructures in One


 

Step Lithography, *J. Micromech. Microeng.*, 2009, **19**, 055003.
61 J. M. Fernandez-Pradas, D. Serrano and P. Serra, Laser Fabricated Microchannels Inside Photostructurable Glass-ceramic, *Appl. Surf. Sci.*, 2009, **255**, 5499–5502.
62 M. J. Madou, *Fundamentals of Microfabrication*, CRC Press, Boca Raton, FL, 2nd edn, 2002.
63 D. Lai, J. M. Labuz, J. Kim, G. D. Luker, A. Shikanov and S. Takayama, Simple Multi-Level Microchannel Fabrication by Pseudo-Grayscale Backside Diffused Light Lithography, *RSC Adv.*, 2013, **3**, 19467–19473.
64 M. Nadasan and A. Manea, Design and Fabrication of the Microchannels for Microfluidics Applications, *U.P.B. Sci. Bull.*, 2009, **71**, 125–134.
65 J. C. McDonald, D. C. Duffy and J. R. Anderson, Fabrication of Microfluidic Systems in Poly (dimethylsiloxane), *Electrophoresis*, 2000, **21**, 27–40.
66 M. Abdelgawad, C. Wu and W. Y. Chien, A Fast and Simple Method to Fabricate Circular Microchannels in Polydimethylsiloxane (PDMS), *Lab Chip*, 2011, **11**, 545–551.
67 P. Yao, G. J. Schneider and D. W. Prather, Three Dimensional Lithographical Fabrication of Microchannels, *J. Microelectromech. Syst.*, 2005, **S14**, 799–805.
68 S. Choi and J.-K. Park, Two Steps Photolithography to Fabricate Multilevel Microchannels, *Biomicrofluidics*, 2010, **4**, 046503.
69 R. Arayanarakool, S. Le Gac and A. van den Berg, Low-temperature, Simple and Fast Integration Technique of Microfluidic Chips by Using a UV-Curable Adhesive, *Lab Chip*, 2010, **10**, 2115–2121.
70 Y. Xia and G. M. Whitesides, Soft Lithography, *Annu. Rev. Mater. Sci.*, 1998, **28**, 153–184.
71 H. Becker and L. E. Locascio, Polymer Microfluidic Devices, *Talanta*, 2002, **56**, 267–287.
72 K. Ueno, F. Kitagawa and H. B. Kim, Fabrication and Characteristic Responses of Integrated Microelectrodes in Polymer Channel Chip, *Chem. Lett.*, 2000, **29**, 858–859.
73 I. Brodie and J. J. Murray, *The Physics of Microfabrication*, Plenum Press, New York, 1982.
74 E. Delamarche, A. Bernard and H. Schmid, Microfluidic Networks for Chemical Patterning of Substrates: Design and Application to Bioassays, *J. Am. Chem. Soc.*, 1998, **120**, 500–508.
75 M. S. Thomas, B. Millare, J. M. Clift, D. Bao, C. Hong and V. I. Vullev, Print-and-Peel Fabrication for Microfluidics: What's in It for Biomedical Applications?, *Ann. Biomed. Eng.*, 2010, **38**, 21–32.
76 A. W. Martinez, S. T. Phillips, M. J. Butte and G. M. Whitesides, Patterned Paper as a Platform for Inexpensive, Low-Volume, Portable Bioassays, *Angew. Chem., Int. Ed.*, 2007, **46**, 1318–1320.
77 A. W. Martinez, S. T. Phillips, E. Carrilho, S. W. Thomas, H. Sindi and G. M. Whitesides, Simple Telemedicine for Developing Regions: Camera Phones and Paper-Based Microfluidic Devices for Real-Time, Off-Site Diagnosis, *Anal. Chem.*, 2008, **80**, 3699–3707.
78 A. W. Martinez, S. T. Phillips, B. J. Wiley, M. Gupta and G. M. Whitesides, FLASH, A Rapid Method for Prototyping Paper-Based Microfluidic Devices, *Lab Chip*, 2008, **8**, 2146–2150.
79 A. W. Martinez, S. T. Phillips, G. M. Whitesides and E. Carrilho, Diagnostics for the Developing World: Microfluidic Paper-Based Analytical Devices, *Anal. Chem.*, 2010, **82**, 3–10.
80 D. A. Bruzewicz, M. Reches and G. M. Whitesides, Low-cost Printing of Poly(dimethylsiloxane) Barriers to Define Microchannels in Paper, *Anal. Chem.*, 2008, **80**, 3387–3392.
81 E. Carrilho, A. W. Martinez and G. M. Whitesides, Understanding Wax Printing: A Simple Micropatterning Process for Paper-based Microfluidics, *Anal. Chem.*, 2009, **81**, 7091–7095.
82 E. Carrilho, S. T. Phillips, S. J. Vella, A. W. Martinez and G. M. Whitesides, Paper Microzone Plates, *Anal. Chem.*, 2009, **81**, 5990–5998.
83 K. M. Schilling, A. L. Lepore, J. A. Kurian and A. W. Martinez, Fully Enclosed Microfluidic Paper-Based Analytical Devices, *Anal. Chem.*, 2012, **84**, 1579–1585.
84 C. Cheng, A. W. Martinez, J. Gong, C. R. Mace, S. T. Phillips, E. Carrilho, K. A. Mirica and G. M. Whitesides, Paper-based ELISA, *Angew. Chem.*, 2010, **122**, 4881–4884.
85 F. A. Gomez, Paper Microfluidics in Bioanalysis, *Bioanalysis*, 2014, **6**, 2911–2914.
86 J. Nie, Y. Liang, Y. Zhang, L. Shangwang, D. Li and S. Zhang, One-Step Patterning of Hollow Microstructures in Paper by Laser Cutting to Create Microfluidic Analytical Devices, *Analyst*, 2013, **138**, 671–676.
87 C. G. Shi, X. Shan, Z. Q. Pan, J. J. Xu, C. Lu, N. Bao and H. Y. Gu, Quantum Dot (QD)-Modified Carbon Tape Electrodes for Reproducible Electrochemiluminescence (ECL) Emission on a Paper-Based Platform, *Anal. Chem.*, 2012, **84**, 3033–3038.
88 C. Renault, J. Koehne, A. J. Ricco and R. M. Crooks, Three-Dimensional Wax Patterning of Paper Fluidic Devices, *Langmuir*, 2014, **30**, 7030–7036.
89 I. Jang and S. Song, Facile and Precise Flow Control for A Paper-Based Microfluidic Device Through Varying Paper Permeability, *Lab Chip*, 2015, **15**, 3405–3412.
90 I. M. Ferrer, H. Valadez, L. Estala and F. A. Gomez, Paper Microfluidic-Based Enzyme Catalyzed Double Microreactor, *Electrophoresis*, 2014, **35**, 2417–2419.
91 J. L. Delaney, C. F. Hogan, J. F. Tian and W. Shen, Electrogenerated Chemiluminescence Detection in Paper-Based Microfluidic Sensors, *Anal. Chem.*, 2011, **83**, 1300–1306.
92 X. Li, J. Tian, T. Nguyen and W. Shen, Paper-Based Microfluidic Devices by Plasma Treatment, *Anal. Chem.*, 2008, **80**, 9131–9134.
93 G. Chitnis, Z. W. Ding, C. L. Chang, C. A. Savranacde and B. Ziaie, Laser-Treated Hydrophobic Paper: An Inexpensive Microfluidic Platform, *Lab Chip*, 2011, **11**, 1161–1165.

94 E. M. Fenton, M. R. Mascareñas, G. P. Lopez and S. S. Sibbett, Multiplex Lateral-Flow Test Strips Fabricated by Two-Dimensional Shaping, *ACS Appl. Mater. Interfaces*, 2009, **1**, 124–129.

95 C. Gallibu, C. Gallibu, A. Avoundjian and F. A. Gomez, Easily Fabricated Microfluidic Devices Using Permanent Marker Inks for Enzyme Assays, *Micromachines*, 2016, **7**(1), 6.

96 A. A. Weaver, H. Reiser, T. Barstis, M. Benvenuti, D. Ghosh, M. Hunckler, B. Joy, L. Koenig, K. Raddell and M. Lieberman, Paper Analytical Devices for Fast Field Screening of Beta Lactam Antibiotics and Antituberculosis Pharmaceuticals, *Anal. Chem.*, 2013, **85**, 6453–6460.

97 C. Renault, X. Li, S. E. Fosdick and R. M. Crooks, Hollow-Channel Paper Analytical Devices, *Anal. Chem.*, 2013, **85**, 7976–7979.

98 K. Scida, B. Li, A. D. Ellington and R. M. Crooks, DNA Detection Using Origami Paper Analytical Devices, *Anal. Chem.*, 2013, **85**, 9713–9720.

99 P. Wang, L. Ge, S. Ge, J. Yu, M. Yan and J. Huang, A Paper-Based Phtoelectrochemical Immunoassay for Low-Cost and Multiplexed Point-Of-Care Testing, *Chem. Commun.*, 2013, **49**, 3294–3296.

100 J. Brugger, R. A. Buser and N. F. D. Rooij, Silicon Cantilevers and Tips for Scanning Force Microscopy, *Sens Actuators, A*, 1992, **34**, 193–200.

101 E. Belloy, S. Thurre and E. Walckiers, The Introduction of Powder Blasting for Sensors and Microsystem Applications, *Sens. Actuators, A*, 2000, **84**, 330–337.

102 J.-H. Park, N.-E. Lee and J. Lee, Deep Dry Etching of Borosilicate Glass Using $SF_6$ and $SF_6$/Ar Inductively Coupled Plasma, *Microelectron. Eng.*, 2005, **8**, 119–128.

103 Yi. Qin, *Micro-manufacturing Engineering and Technology*, Elsevier Inc., Oxford, 1st edn, 2010.

104 M. Hakamada, Y. Asao, T. Kuromura, Y. Chen, H. Kusuda and M. Mabuchi, Fabrication of Copper Microchannels by the Spacer Method, *Scr. Mater.*, 2007, **56**, 781–783.

105 M. K. S. Verma, A. Majumder and A. Ghatak, Embedded Template-assisted Fabrication of Complex Microchannels in PDMS and Design of a Microfluidic Adhesive, *Langmuir*, 2006, **22**, 10291–10295.

106 A. Lamberti, Microfluidic Photocatalytic Device Exploiting PDMS/$TiO_2$ Nanocomposite, *Appl. Surf. Sci.*, 2015, **335**, 50–54.

107 Z. Han, J. Li, W. He, S. Li, Z. Li, J. Chu and Y. Chen, A Microfluidic Device with Integrated ZnO Nanowires for Photodegradation Studies of Methylene Blue under Different Conditions, *Microelectron. Eng.*, 2013, **111**, 199–203.

108 M. Rasponi, T. Ullah, R. J. Gilbert, G. B. Fiore and T. A. Thorsen, Realization and Efficiency Evaluation of a Micro-Photocatalytic Cell Prototype for Real-time Blood Oxygenation, *Med. Eng. Phys.*, 2011, **33**(7), 887–892.

109 H. Eskandarloo and A. Badiei, Fabrication of an Inexpensive and High Efficiency Microphotoreactor Using $CO_2$ Laser Technique for Photocatalytic Water Treatment Applications, *Environ. Technol.*, 2015, **36**, 1063–1073.

110 H.-J. Koo and O. D. Velev, Biomimetic Photocatalytic Reactor with a Hydrogel-Embedded Microfluidic Network, *J. Mater. Chem. A*, 2013, **1**, 11106–11110.

111 G. Charles, T. Roques-Carmes, N. Becheikh, L. Falk, J.-M. Commenge and S. Corbel, Determination of Kinetic Constants of a Photocatalytic Reaction in Micro-Channel Reactors in the Presence of Mass-transfer Limitation and Axial Dispersion, *J. Photochem. Photobiol., A*, 2011, **223**, 202–211.

112 S. Corbel, G. Charles, N. Becheikh, T. Roques-Carmes and O. Zahraa, Modelling and Design of Microchannel Reactor for Photocatalysis, *Virtual Phys. Prototyp.*, 2012, **7**, 203–209.

113 T. H. Yoon, L. Y. Hong and D. P. Kima, Photocatalytic Reaction Using Novel Inorganic Polymer Derived Packed Bed Microreactor with Modified $TiO_2$ Microbeads, *Chem. Eng. J.*, 2011, **167**, 666–670.

114 L. Lei, N. Wang, X. M. Zhang, Q. Tai, D. P. Tsai and H. L. W. Chan, Optofluidic Planar Reactors for Photocatalytic Water Treatment Using Solar Energy, *Biomicrofluidics*, 2010, **4**, 043004.

115 H. Lindstrom, R. Wootton and A. Iles, High Surface Area Titania Photocatalytic Microfluidic Reactors, *AIChE J.*, 2007, **53**, 695–702.

116 B. Ramos, S. Ookawara, Y. Matsushita and S. Yoshikawa, Photocatalytic Decolorization of Methylene Blue in a Glass Channel Microreactor, *J. Chem. Eng. Jpn.*, 2014, **47**, 788–791.

117 Z. He, Y. Li, Q. Zhang and H. Wanga, Capillary Microchannel-based Microreactors with Highly Durable ZnO/$TiO_2$ Nanorod Arrays for Rapid, High Efficiency and Continuous-Flow Photocatalysis, *Appl. Catal., B*, 2010, **93**, 376–382.

118 X. Li, H. Wang, K. Inoue, M. Uehara, H. Nakamura, M. Miyazaki, E. Abea and H. Maeda, Modified Microspace Using Self-Organized Nanoparticles for Reduction of Methylene Blue, *Chem. Commun.*, 2003, **2003**, 964–965.

119 H. Nakamura, X. Li, H. Wang, M. Uehara, M. Miyazaki, H. Shimizu and H. Maeda, A Simple Method of Self-Assembled Nano-Particles Deposition on the Micro-Capillary Inner Walls and the Reactor Application for Photocatalytic and Enzyme Reactions, *Chem. Eng. J.*, 2004, **101**, 261–268.

120 K. Oda, Y. Ishizaka, T. Sato, T. Eitoku and K. Katayama, Analysis of Photocatalytic Reactions Using a $TiO_2$ Immobilized Microreactor, *Anal. Sci.*, 2010, **26**, 969–972.

121 Y. Yamada, M. Mizutani, T. Nakamura and K. Yano, Mesoporous Microcapsules with Decorated Inner Surface: Fabrication and Photocatalytic Activity, *Chem. Mater.*, 2010, **22**, 1695–1703.

122 Y. Matsushita, N. Ohbab, S. Kumadab, K. Sakeda, T. Suzuki and T. Ichimura, Photocatalytic Reactions in Microreactors, *Chem. Eng. J.*, 2008, **135S**, S303–S308.

123 M. Krivec, K. Zagar, L. Suhadolnik, M. Ceh and G. Drazic, Highly Efficient $TiO_2$ Based Microreactor for Photocatalytic Applications, *ACS Appl. Mater. Interfaces*, 2013, **5**, 9088–9094.


 

124 H. Eskandarloo, A. Badiei, M. A. Behnajady and G. M. Ziarani, UV-LEDs Assisted Preparation of Silver Deposited $TiO_2$ Catalyst Bed Inside Microchannels as A High Efficiency Microphotoreactor for Cleaning Polluted Water, *Chem. Eng. J.*, 2015, **270**, 158–167.
125 H. C. Aran, D. Salamon, T. Rijnaarts, G. Mul, M. Wessling and R. G. H. Lammertink, Porous Photocatalytic Membrane Microreactor (P2M2): A New Reactor Concept for Photochemistry, *J. Photochem. Photobiol., A*, 2011, **225**, 36–41.
126 S. Teekateerawej, J. Nishino and Y. Nosaka, Design and Evaluation of Photocatalytic Micro-Channel Reactors Using $TiO_2$-Coated Porous Ceramics, *J. Photochem. Photobiol., A*, 2006, **179**, 263–268.
127 S. Teekateerawej, J. Nishino and Y. Nosaka, Photocatalytic Microreactor Study Using $TiO_2$-Coated Porous Ceramics, *J. Appl. Electrochem.*, 2005, **35**, 693–697.
128 R. Gorges, S. Meyer and G. Kreisel, Photocatalysis in Microreactors, *J. Photochem. Photobiol., A*, 2004, **167**, 95–99.
129 S. Corbel, N. Becheikh, T. Roques-Carmes and O. ZahraaL, Mass Transfer Measurements and Modeling in a Microchannel Photocatalytic Reactor, *Chem. Eng. Res. Des.*, 2014, **92**, 657–662.
130 B.-C. Choi, L.-H. Xu, H.-T. Kim and D. W. Bahnemann, Photocatalytic Characteristics on Sintered Glass and Microreactor, *J. Ind. Eng. Chem.*, 2006, **12**, 663–672.
131 M. Gao, Z. Zeng, B. Sun, H. Zou, J. Chen and L. Shao, Ozonation of Azo Dye Acid Red 14 in A Microporous Tube-In-Tube Microchannel Reactor: Decolorization and Mechanism, *Chemosphere*, 2012, **89**, 190–197.
132 M. Saquib and M. Muneer, $TiO_2$–Photocatalytic Degradation of a Triphenyl Methane Dye (gentian violet), in Aqueous Suspensions, *Dyes Pigm.*, 2003, **56**, 37–49.
133 S. Sakthivel, B. Neppolian, M. V. Shankar, B. Arabindoo, M. Palanichamy and V. Murugesan, Solar Photocatalytic Degradation of Azo Dye: Comparison of Photocatalytic Efficiency of ZnO and $TiO_2$, *Sol. Energy Mater. Sol. Cells*, 2003, **77**, 65–82.
134 D. N. Priya, J. M. Modak, P. Trebse, R. Zabar and A. M. Raichur, Photocatalytic Degradation of Dimethoate Using LbL Fabricated $TiO_2$/Polymer Hybrid Films, *J. Hazard. Mater.*, 2011, **195**, 214–222.
135 C. G. Silva and J. L. Faria, Effect of Key Operational Parameters on the Photocatalytic Oxidation of Phenol by Nanocrystalline Sol–Gel $TiO_2$ under UV Irradiation, *J. Mol. Catal. A: Chem.*, 2009, **305**, 147–154.
136 S. Ahmed, M. G. Rasul, W. N. Martens, R. Brown and M. A. Hashib, Advances in Heterogeneous Photocatalytic Degradation of Phenols and Dyes in Wastewater: A Review, *Water, Air, Soil Pollut.*, 2011, **215**, 3–29.
137 Z. Shourong, H. Qingguo, Z. Jun and W. Bingkun, A Study on Dye Photoremoval in $TiO_2$ Suspension Solution, *J. Photochem. Photobiol., A*, 1997, **108**, 235–238.
138 M. S. T. Conçalves, A. M. F. Oliveira-Campos, M. M. S. Pinto, P. M. S. Plasencia and M. J. R. P. Queiroz, Photochemical Treatment of Solutions of Azo Dyes Containing $TiO_2$, *Chemosphere*, 1999, **39**, 781–786.
139 C. Galindo, P. Jacques and A. Kalt, Photodegradation of the Aminoazo Benzene Acid Orange 52 by Three Advanced Oxidation Processes : $UV/H_2O_2$, $UV/TiO_2$ and $VIS/TiO_2$ Comparative Mechanistic and Kinetic Investigations, *J. Photochem Photobiol., A*, 2000, **130**, 35–47.
140 A. Sharma, P. Rao, R. P. Mathur and S. C. Ametha, Photocatalytic Reactions of Xylidine Ponceau on Semiconducting Zinc Oxide Powder, *J. Photochem. Photobiol., A*, 1995, **86**, 197–200.
141 S. Sakthivel, B. Neppolian, M. Palanichamy, B. Arabindoo and V. Murugesan, Photocatalytic Degradation of Leather Dye, Acid Green 16 Using ZnO in the Slurry and Thin Film Forms, *Indian J. Chem. Technol.*, 1999, **6**, 161–165.
142 N. Daneshvar, M. Rabbani, N. Modirshahla and M. A. Behnajady, Photooxidative Degradation of Acid Red 27 in a Tubular Continuous-flow Photoreactor: Influence of Operational Parameters and Mineralization Products, *J. Hazard. Mater.*, 2005, **118**, 155–160.
143 M. A. Behnajady and Y. Tohidi, The Effect of Operational Parameters in the Photocatalytic Activity of Synthesized Mg/ZnO–$SnO_2$ Nanoparticles, *Desalin. Water Treat.*, 2015, **53**, 1335–1341.
144 S. Aber, H. Mehrizade and A. R. Khataee, Preparation of ZnS Nanocrystal and Investigation of its Photocatalytic Activity in Removal of CI Acid Blue 9 from Contaminated Water, *Desalin. Water Treat.*, 2011, **28**, 92–96.
145 A. A. Khodja, T. Sehili, J. F. Pilichowski and P. Boule, Photocatalytic Degradation of 2- Phenylphenol on $TiO_2$ and ZnO in Aqueous Suspensions, *J. Photochem. Photobiol., A*, 2001, **141**, 231–239.
146 D. Dong, P. Li, X. Li, Q. Zhao, Y. Zhang, C. Jia and P. Li, Investigation on the Photocatalytic Degradation of Pyrene on Soil Surfaces Using Nanometer Anatase $TiO_2$ under UV Irradiation, *J. Hazard. Mater.*, 2010, **174**, 859–863.
147 Y. Liu, Z. Wang, B. Huang, Y. Dai, X. Qin and X. Zhang, Microstructure Modulation of Semiconductor Photocatalysts for $CO_2$ Reduction, *Curr. Org. Chem.*, 2014, **18**, 620–628.
148 T. Zhao, Y. Zhao and L. Jiang, Nano-/Microstructure Improved Photocatalytic Activities of Semiconductors, *Philos. Trans. R. Soc. London, Ser. A*, 2016, **371**, 1–16.
149 M. Anpo, H. Yamashita, Y. Ichihashi, Y. Fujii and M. Honda, Photocatalytic Reduction of CO2 with H2O on Titanium Oxides Anchored with Micropores of Zeolites: Effects of the Structure of the Active Sites and the Addition of Pt, *J. Phys. Chem. B*, 1997, **101**, 2632–2636.
150 G. Lassaletta, A. Fernandez, J. P. Espinos and A. R. Gonzalez-Elipe, Spectroscopic Characterization of Quantum-Sized $TiO_2$ Supported on Silica: Influence of Size and $TiO_2$–$SiO_2$ Interface Composition, *J. Phys. Chem.*, 1995, **99**, 1484–1490.
151 S. H. Tolbert, A. Herhold, C. Johnson and A. Alivisatos, Comparison of Quantum Confinement Effects on the Electronic Absorption Spectra of Direct and Indirect Gap

Semiconductor Nanocrystals, *Phys. Rev. Lett.*, 1994, **73**, 3266–3269.

152 Z. Q. Song, H. Y. Xu, K. W. Li, H. Wang and H. Yan, Hydrothermal Synthesis And Photocatalytic Properties of Titanium Acid $H_2Ti_2O_5 \cdot H_2O$ Nanosheets, *J. Mol. Catal. A: Chem.*, 2005, **239**, 87–91.

153 J. T. McCann, M. Marquez and Y. Xia, Melt Coaxial Electrospinning: A Versatile Method for the Encapsulation of Solid Materials and Fabrication of Phase Change Nanofibers, *Nano Lett.*, 2006, **6**, 2868–2872.

154 C. Xiong and J. K. J. Balkus, Fabrication of $TiO_2$ Nanofibers from a Mesoporous Silica Film, *Chem. Mater.*, 2005, **17**, 5136–5140.

155 S. Das and V. C. Srivastava, Hierarchical nanostructured ZnO-CuO nanocomposite and its photocatalytic activity, *J. Nano Res.*, 2015, **35**, 21–26.

156 P. R. Potti and V. C. Srivastava, Effect of dopants on ZnO mediated photocatalysis of dye bearing wastewater: A Review, in *Engineering Applications of Nanoscience and Nanomaterials*, Mater. Sci. Forum, 2013, vol. 757, pp. 165–174.

157 T. T. Vu, L. del Rıo, T. Valdes-Solıs and G. Marban, Stainless Steel Wiremesh-Supported Zno for The Catalytic Photodegradation of Methylene Blue under Ultraviolet Irradiation, *J. Hazard. Mater.*, 2013, **246–247**, 126–134.

158 S. Sohrabnezhad, A. Pourahmad and E. Radaee, Photocatalytic Degradation of Basic Blue 9 By Cos Nanoparticles Supported on Almcm-41 Material As a Catalyst, *J. Hazard. Mater.*, 2009, **170**, 184–190.

159 F. Li, S. Sun, Y. Jiang, M. Xia, M. Sun and B. Xue, Photodegradation of an Azo Dye Using Immobilized Nanoparticles of $TiO_2$ Supported by Natural Porous Mineral, *J. Hazard. Mater.*, 2008, **152**, 1037–1044.

160 X. Qiu, Z. Fang, B. Liang, F. Gu and Z. Xu, Degradation of Decabromodiphenyl Ether by Nano Zero-Valent Iron Immobilized in Mesoporous Silica Microspheres, *J. Hazard. Mater.*, 2011, **193**, 70–81.

161 M. S. Lucas, P. B. Tavares and J. A. Peres, Photocatalytic Degradation of Reactive Black 5 with $TiO_2$-Coated Magnetic Nanoparticles, *Catal. Today*, 2013, **209**, 116–121.

162 R. Shao, L. Sun, L. Tang and Z. Chen, Preparation and Characterization of Magnetic Core-Shell $ZnFe_2O_4$@ZnO Nanoparticles and Their Application for the Photodegradation of Methylene Blue, *Chem. Eng. J.*, 2013, **217**, 185–191.

163 J. Theurich, M. Lindner and D. W. Bahnemann, Photocatalytic Degradation of 4-chlorophenol in Aerated Aqueous Titanium Dioxide Suspensions: A Kinetic and Mechanistic Study, *Langmuir*, 1996, **12**, 6368–6376.

 